HHS Public Access

Author manuscript

*Langmuir*. Author manuscript; available in PMC 2019 June 11.

Published in final edited form as:

*Langmuir*. 2016 March 15; 32(10): 2450–2457. doi:10.1021/acs.langmuir.5b04332.

# Oxidation of Membrane Curvature-Regulating Phosphatidylethanolamine Lipid Results in Formation of Bilayer and Cubic Structures

**Shalene Sankhagowit**[†], **Ernest Y. Lee**[‡], **Gerard C. L. Wong**[‡], and **Noah Malmstadt**[*,†]

[†]Mork Family Department of Chemical Engineering and Materials Science, University of Southern California, Los Angeles, California 90089, United States

[‡]Bioengineering Department, Chemistry & Biochemistry Department, California Nano Systems Institute, University of California, Los Angeles, California 90095, United States

## Abstract

Oxidation is associated with conditions related to chronic inflammations and aging. Cubic structures have been observed in the smooth endoplasmic reticulum and mitochondrial membranes of cells under oxidative stress (e.g., tumor cells and virus-infected cells). It has been previously suspected that oxidation can result in the rearrangement of lipids from a fluid lamellar phase to a cubic structure in organelles containing membranes enriched with amphiphiles that have nonzero intrinsic curvature, such as phosphatidylethanolamine (PE) and cardiolipin. This study focuses on the oxidation of 1,2-dioleoyl-*sn*-glycero-3-phosphoethanolamine (DOPE), a lipid that natively forms an inverted hexagonal phase at physiological conditions. The oxidized samples contain an approximately 3:2 molar ratio of nonoxidized to oxidized DOPE. Optical microscopy images collected during the hydration of this mixture from a dried film suggest that the system evolves into a coexistence of a stable fluid lamellar phase and transient square lattice structures with unit cell sizes of 500–600 nm. Small-angle X-ray scattering of the same lipid mixture yielded a body-centered Im3m cubic phase with the lattice parameter of 14.04 nm. On average, the effective packing parameter of the oxidized DOPE species was estimated to be 0.657 ± 0.069 (standard deviation). This suggests that the oxidation of PE leads to a group of species with inverted molecular intrinsic curvature. Oxidation can create amphiphilic subpopulations that potently impact the integrity of the membrane, since negative Gaussian curvature intrinsic to cubic phases can enable membrane destabilization processes

## Graphical Abstract

[*]**Corresponding Author** malmstad@usc.edu. Phone: +1 213 821 2034. Fax: +1 213 740 1056.

ASSOCIATED CONTENT

Supporting Information

The Supporting Information is available free of charge on the ACS Publications website at DOI: 10.1021/acs.langmuir.5b04332. Optical micrographs of DOPC and DOPE; profiles of the reflection signal corresponding to reciprocal lattice vectors *a** and *b**; relative amounts of total oxidized (filled circles) and peroxidized (open squares) DOPE with duration of oxidation; and fluorescence emission of DOPE and DOPC samples (PDF)

Notes

The authors declare no competing financial interest.

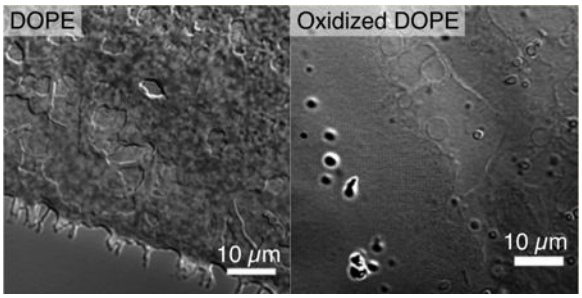


## INTRODUCTION

Lipids in cellular membranes can exist in a fluid lamellar ($L_\alpha$) phase, forming a planar bilayer morphology as depicted in the fluid mosaic model.[1] Nonlamellar lipid structures can exist, and are often associated with dynamic cellular processes. In the inverted hexagonal ($H_{II}$) phase, lipid molecules arrange into cylinders with the head groups oriented inward in contact with the aqueous phase core.[2] Lipids that form the $H_{II}$ phase have been observed at higher concentrations in intermediate structures during membrane fusion in model membranes and in cells.[3–5] The inverted cubic ($Q_{II}$) phase consists of lipids arranged into minimal surfaces.[6] It is periodic in three dimensions and creates two discrete networks of water channels.[7] The $Q_{II}$ phase has been observed during plasma membrane folding through nonclathrin mediated endocytosis.[8] Cubic phases have been previously associated with smooth endoplasmic reticulum (ER) and certain states of inner mitochondrial (MT) membranes.[8,9]

A variety of terms, including “undulating membrane”[10] and “tubuloreticular structures”,[8,11] have been applied to cubic phase structures that have been regarded as potential ultrastructural markers for cellular stresses.[12] They have been observed in smooth ER membranes of severe acute respiratory syndrome (SARS)-infected cells[13] and tumor cells in various organs.[10] One of the most well characterized *in vivo* cases of cubic phase formation results from the morphological transition of the inner MT membrane upon food depletion in the giant amoeba *Chaos carolinensis*.[12] The progressive formation of the cubic phase was accompanied by increasing levels of the reactive oxygen species (ROS) superoxide and hydrogen peroxide, resulting from changes in oxidative metabolism of the organism upon starvation.[14] It is important to note that these studies reported cubic phase formation in smooth ER and inner MT membranes that contain highly folded membranes with high concentrations of lipids with nonzero intrinsic curvature.[9,15–17]

Approximately half of the phospholipids comprising the highly folded and compartmentalized inner MT membrane in mammalian cells are curvature-regulating phosphatidylethanolamine (PE) and cardiolipin species.[17] These lipids are found in particularly high concentrations at the contact sites between inner and outer mitochondrial membranes. They likely play a role in protein import and phospholipid translocation between the two layers of the organelle.[18,19] It has also been shown that PE lipids facilitate formation of membrane fusion intermediate structures[3,4] and support cytokinesis during cell division.[20]

The ability of PE lipids to support high membrane curvatures for routine cell functions and division arises from their molecular structures. PE lipids have a smaller headgroup relative to the cross-sectional area of the hydrocarbon tails than phosphatidylcholine (PC) lipids that comprise the majority of phospholipids. Lipid molecules that support formation of the lamellar phases in the bilayer membrane, such as PC lipids, have comparable lateral areas in the head and tail regions and have an overall cylindrical molecular geometry. For phospholipids in general, the ratio of head-to-tail area is temperature dependent, with the area occupied by the tail groups increasing with temperature.[21] Above the phase transition temperature ($T_h$), a PE lipid can have an anisotropic wedge shape: it looks fan-shaped (hydrophobic region wider that the headgroup) in the plane that contains the centers of mass of the two alkyl chains; however, perpendicular to this plane, the shape is much less anisotropic.[22] This wedge shape supports the formation of the $H_{II}$ phase. Our study focuses on the lipid 1,2-dioleoyl-*sn*-glycero-3-phosphoethanolamine (DOPE) that transforms from the bilayer-forming fluid lamellar phase ($L_\alpha$) to the $H_{II}$ phase as temperature increases across $T_h = 13$ °C.[23]

Oxidation alters lipid molecular structures and can disrupt PE lipid functionality. Much of the endogenous sources of ROS that can initiate oxidation of the bilayer membrane arise as byproducts and downstream products of cellular metabolism.[24] Electron leakages from the electron transport chain at the inner mitochondrial membrane lead to the formation of superoxide that is a ROS itself and a precursor to many others.[25] While many products can form upon oxidation of the lipid bilayer, the typical result involves scission of an unsaturated hydrocarbon tail and/or the addition of a polar group to the same chain.[26] The common consequence is the loss of a portion of the hydrophobic moiety, either to the hydrophilic region or by removal from the bilayer into the aqueous phase.[27] This results in a subpopulation with a reduction of the negative intrinsic curvature. Oxidation threatens lipid functionality with alterations to molecular structure that control membrane fluidity, permeability, and topology.[27,28]

In this study, we used optical microscopy to observe the hydration of oxidized DOPE lipid films at room temperature. With the addition of water, the lipid film swelled to form micron-scale lamellar phase structures that included elongated tubules and spherical vesicles. In contrast, the nonoxidized, $H_{II}$ phase DOPE shows no apparent changes upon hydration to the lipid film at this length-scale. Using the same viewing technique, we saw formation of submicron-scale lattice structures that are stable for up to 3 h. Characterization of 2-D projections in optical micrographs with a 2-D discrete fast Fourier transform (FFT) revealed that such lattices resemble highly swollen periodic structures, with the square unit lattice parameter on the order of hundreds of nanometers. Small-angle X-ray scattering (SAXS) in general cannot access micron scale ordering in weakly scattering structures, such as those depicted in the micrographs here. However, SAXS can assay unambiguously the existence of cubic phases. Using SAXS, we find that oxidized DOPE can form a 3-D Im3m cubic phase with a lattice parameter of 14.04 nm, which indicates that the DOPE oxidation process has enhanced the system's ability to form negative Gaussian curvature, the type of curvature topologically required for membrane permeation processes.[29]

Lipid membranes in $Q_{II}$ phases can be formed *in vitro* with monoacylglycerides to provide 3-D periodic structures for protein crystallization.[30,31] Cubic phases have also been shown to emerge after temperature cycling DOPE (as well as its monomethylated analog, DOPE-Me) across its phase transition temperature hundreds of times.[32,33] The lattice parameters of these cubic phase structures range between tens and hundreds of angstroms and are tunable with either lipid or aqueous phase composition.[31,34,35] The largest reported stable cubic phase lattice parameter so far is 470 Å, and transient cubic structures have been formed at 300–400 Å.[36] Although chain packing does not permit the formation of cubic phases based on minimal surfaces at these large length-scales, it is interesting that DOPE oxidation apparently drives the generation of lipid structures with periodic symmetry, and does so at length-scales comparable to those of cubic structures observed *in vivo*.[10,12,37]

It has been previously hypothesized that membrane lipids can be structured into the cubic phase by oxidative damage.[12] We quantified the extent of oxidation with nuclear magnetic resonance (NMR) spectroscopy in order to estimate the effective molecular shape of the collective oxidation product species that could support bilayer formation. We then observed hydrated films of nonoxidized DOPE with various concentrations of a lyso-PE lipid in order to mimic the process of tail group area reduction that occurs with oxidation. None of the combinations between $H_{II}$ phase and micelle formation yielded lattice structures that are observable with optical microscopy. Our results suggest that the cubic structure formation in oxidized DOPE results from molecular alterations that affect lipid packing beyond changes to head-to-tail group area ratios.

## EXPERIMENTAL SECTION

### Materials.

The lipids 1,2-dioleoyl-*sn*-glycero-3-phosphoethanolamine (DOPE), 1,2-dioleoyl-*sn*-glycero-3-phosphocholine (DOPC), and 1-oleoyl-2-hydroxy-*sn*-glycero-3-phosphoethanolamine (lyso-PE) were purchased from Avanti Polar Lipids. Chloroform was from Macron Fine Chemicals, and deuterated chloroform was from Cambridge Isotope Laboratories, Inc.

### Oxidation of DOPE.

DOPE was oxidized while dried and exposed to air. Heat was applied to accelerate the oxidation process. For each DOPE sample, 1 mL of the lipid solution at 10 mg/mL in chloroform was dried on a glass Petri dish (60 × 15 mm, VWR) with an argon stream and stored under vacuum for 90 min. For each 4-h interval of oxidation, the lipid film-lined Petri dish was then placed on a hot plate (C-MAG HS 7, IKA) set to 50 °C. Three samples were oxidized in parallel. The Petri dishes were covered to avoid falling contaminants but air exposure was allowed. Outside the 90 min dry time under vacuum and 4-h oxidation time on the hot plate, the lipid samples were sealed under an argon environment and stored dissolved in chloroform at −20 °C to avoid unintentional oxidation.

### Hydration of lipid films.

To observe the morphology of a hydrated oxidized DOPE sample, lipid films were prepared by drying 5 μL × 10 mg/mL of the lipid in chloroform as approximately 0.5 μL spots on a round glass coverslip (#1, 25 mm, Chemglass) with a 25 μL glass syringe (Hamilton). The lipids were allowed to dry for at least 90 min under vacuum before the coverslip was placed in a Sykes-Moore viewing chamber (Bellco Glass). Note that nonoxidized DOPE and DOPC samples were also prepared using this protocol, dried with 0.05 mg of lipids on each coverslip.

For the hydration of lyso-PE/DOPE mixtures, 5 μL x 10 mg/mL DOPE was combined with different volumes of 5 or 10 mg/mL lyso-PE solutions to yield 10, 20, 30, 40, 50, 60, 70, 80, 90, and 95 mol % lyso-PE. These solutions were diluted with different amounts of chloroform such that the final concentration of DOPE in each was approximately 0.7 mg/mL. For each mixture, 5 μL was then used to dry approximately 0.5 μL spots on a glass coverslip as described above.

For observation, the edge of a spot of dried lipid film close to the center of the coverslip was located using a Zeiss Axio Observer inverted microscope operating under the differential interference contrast (DIC) mode, with a Plan-Apochromat 20×/0.8 NA objective (lower resolution) or a Plan-Apochromat 63×/1.40 NA oil objective with 1.6× optovar magnification (higher resolution; 15.504 px/μm). The lipid film was hydrated with 500 μL Milli-Q water (Millipore). Note that this high volume was used to maintain hydration at the center of the coverslip while the added water wetted the wall of the viewing chamber.

### SAXS experiments.

Small-angle X-ray scattering (SAXS) experiments were conducted to investigate the structure of oxidized DOPE in solution. Samples were equilibrated for 2 days before measurement. 24-h oxidized DOPE and regular DOPE were solubilized in chloroform at 12.5 and 20 mg/mL, respectively. Individual samples were aliquoted into smaller volumes in glass vials. The chloroform was evaporated from each vial under dry nitrogen gas and the sample was further desiccated overnight under vacuum. After 24 h, Milli-Q water was added for resuspension to 20 mg/mL. Samples were prepared for SAXS by diluting hydrated regular DOPE or oxidized DOPE to 10 mg/mL in Milli-Q water to a total volume of 40 μL. Quartz glass capillaries (Hilgenberg) were loaded with the 40 μL samples and hermetically sealed. Measurements of the samples were made at the Stanford Synchrotron Radiation Lightsource, beamline 4–2. A monochromatic 9 keV X-ray with a 1.7 m path length was used, and samples were exposed for 10 s. Scattered radiation was collected using a Rayonix MX225-HE detector (pixel size, 73.2 μm). 2-D diffraction images were processed and integrated with the Nika 1.68 package for Igor Pro 6.37 and FIT2D. For all samples, several measurements were taken to ensure consistency of data.

### Chemical analysis of oxidized DOPE.

To approximate the extent of oxidation of DOPE tails, the ratio between the amounts of vinyl and glycerol protons obtained from nuclear magnetic resonance (NMR) spectroscopy was determined. The lipid samples (approximately 10 mg) in chloroform were dried onto the

bottom of a glass test tube under an argon stream and further dried under vacuum for at least 90 min before being dissolved in 800 μL deuterated chloroform. If the lipid was already dried on a glass Petri dish (after an oxidation step), then it was directly dissolved into deuterated chloroform. Samples were scanned on a Varian Mercury 400 2-channel NMR spectrometer at 25 °C. Manual phase and baseline correction, as well as integration, were performed using the MNova NMR processing software (Mestrelab Research).

## RESULTS AND DISCUSSION

### Hydration of oxidized DOPE lipid films.

Lipid morphologies were observed using optical microscopy in differential interference contrast (DIC) mode to enhance the edges of structures. The lipid samples were deposited directly onto the glass coverslips used in microscopy for time-course observations of lipid hydration from the dried state. Oxidized DOPE was prepared in 10 mg batches, and oxidation was induced during 4-h intervals for a total of 24 h. To optimize the oxidation process, the lipid was dried onto a glass Petri dish and heated to 50 °C while exposed to ambient air during each 4-h interval. Additionally, each batch was dissolved in chloroform and, again, dried with an argon stream and placed under vacuum for 90 min in between each oxidation interval. This was done to improve product uniformity as oxidation more readily occurred on the surface of the dried lipid film. To avoid unintentional oxidation of the samples, the lipids were stored dissolved in chloroform under an argon environment at −20 °C outside of the 4-h oxidation and 90 min vacuum-drying periods.

For each hydration experiment, a lipid sample in chloroform at 10 mg/mL was applied as approximately 0.5 μL spots with a glass syringe onto the coverslip and placed under vacuum for at least 90 min for solvent removal. For uniformity, the results presented here are of 90 min dried lipid films, although the same results were achieved when the lipid was dried overnight. The coverslip was then placed in a Sykes-Moore viewing chamber for microscopy. A series of micrographs from a time-course observation of oxidized DOPE film hydration is shown in Figure 1. Image capturing was initiated seconds prior to the addition of Milli-Q water to record the dried lipid film (Figure 1A). The lipid film edges are ideal for observation due to higher film thickness made by the coffee ring effect when drying. Note that the area of the film close to the left edge of the micrograph was thicker than in the rest of the image. Within 20 s of hydration, oxidized DOPE formed vesicles, as well as loose and densely packed tubules (Figure 1B, right and left sides, respectively). The latter quickly organized into lattice structures with clusters of periodic domains that spanned tens of microns (Figure 1C, left half). Figure 1C shows coexistence of the $L_{\alpha}$ phase (represented by giant vesicles) and this lattice structure. The lattice was stable for minutes before its transition back into densely packed tubules (Figure 1D, E) that dispersed in both lateral and vertical directions (Figure 1F). Note that structures appearing at higher contrast in Figure 1F were further away from the coverslip and the focal plane was not changed. The duration at which the lattice structure appears, from minutes to an hour, varied based on the concentration of the lipid solution in chloroform during film preparation. Higher concentrations yielded thicker lipid films and resulted in longer-lived latticed structures (Figure S1).

Figure S2 compares another oxidized DOPE film in the dried state and at 5 min after hydration, observed under lower magnification. At this length-scale, the lattice structure appears as nebulous clusters with indistinct boundaries. Additionally, high contrast globular structures were present from the beginning of the hydration period (Figure 1B–F and Figure S2B) and increased in numbers upon the transition of the lattice structure to tubules and vesicles (Figure 1F).

For comparison with $L_\alpha$ and $H_{II}$ phases, the hydration experiment was repeated using DOPC and nonoxidized DOPE, respectively (Figure 2 at higher magnification and Figure S3 at lower magnification). DOPC is a phospholipid commonly used in the laboratory to form $L_\alpha$ phase structures.[38,39] After 5 min of hydration, the DOPC lipid molecules at the surface of the film had swelled into vesicles and tubules (Figure 2B and Figure S3B). Hydrated DOPE is expected to form the $H_{II}$ phase in the aqueous environment,[23] which is not optically resolvable. No formation of lamellar phase structures was observed 5 min after hydration (Figure 2D). An exception is the presence of several tubules formed at the edge of the DOPE film in Figure S3D (arrow and inset). The chemical analysis of lipid samples, presented later in this work, shows low levels of oxidation prior to the first 4-h round of exposure to air and heat. Immediately upon hydration, rearrangements within the DOPE film occurred that resulted in an apparently more compact film with receded edges. Under the same observation resolution used to view images in Figure 1, the lattice structure observed in hydrated oxidized DOPE was not seen in either the DOPC or nonoxidized DOPE samples.

### Analysis of the lattice structure.

To characterize the lattice structure formed with hydrated oxidized DOPE, we applied a 2-D discrete fast Fourier transform (FFT) to visualize the 2-D projections of micrograph images in the frequency domain. A section cropped from a larger micrograph was used for FFT analysis in order to extract information only pertaining to the lattice structure. Due to the large number of structured domains that can be captured in the images, we assume that we have data at different orientations of the same structure. The micrograph in Figure 3A shows the lattice structure with a box indicating the cropped section used in the analysis; the resulting frequency domain image is shown in Figure 3B. The reciprocal lattice vectors $a^*$ and $b^*$ in Figure 3B correspond to lattice parameters $a = 625 \pm 202$ nm (standard deviation of the Gaussian function fitted to the reflection signal, Figure S4) and $b = 628 \pm 217$ nm, and the angle between the means of the reflection signal is 90°. Figure 3B indicates that hydrated oxidized DOPE forms a transitional square lattice system with unit cell sizes close to half of a micron. Similarly, the structure in Figure 1C has lattice parameters $a = 304 \pm 35$ nm and $b = 309 \pm 68$ nm (Figure S5).

We attempted to characterize the lattice structure in the zdimension and collected image stacks of the same x-y location at multiple focal planes set to 0.01 $\mu$m intervals, spanning at least 4 $\mu$m. By reconstructing the image as x-z and y-z cross sections of the image stack, the lattice intervals ($a = 574 \pm 135$ nm and $b = 574 \pm 178$ nm) seen in the $x$–$y$ plane continued in the $z$-direction (Figure S6A). However, the lattice spacing in the $z$-direction could not be resolved. Taken together, these data suggest that large structures with square symmetry can be made in the oxidation process.

To determine whether oxidized DOPE can form a stable 3-D cubic phase structure, we utilized SAXS.[40,41] We find that oxidized DOPE forms an Im3m body-centered cubic lattice with a lattice parameter of $a$ = 14.04 nm (Figure 4, yellow). Three peaks are observed at $q$ = 0.063, 0.090, and 0.110 Å $^{-1}$, which index to a ratio of $\sqrt{2}:\sqrt{4}:\sqrt{6}$. Higher order reflections are also observed at $\sqrt{10}:\sqrt{12}:\sqrt{14}$, corresponding to $q$ = 0.142, 0.154, 0.16. The magnitude of negative Gaussian curvature of this phase is $\langle k \rangle = 2\pi\chi/A_0 d^2 = -5.4 \times 10^{-4}$ Å$^{-2}$, where $\chi = -4$ and $A_0 = 2.345$. Note that low intensity peaks for the Pn3m phase group with the lattice parameter of 10.8 nm were also observed. For comparison, the sample prepared with nonoxidized DOPE showed inverted hexagonal phase characteristics with a lattice constant of $a$ = 7.46 nm (Figure 4, blue), which is consistent with values found in the literature.[42]

Three inverted cubic phases supported by lipid species have been reported: primitive (Im3m), double diamond (Pn3m), and gyroid (Ia3d). A commonly fabricated lipidic cubic phase structure is composed of 1-oleoyl-*rac*-glycerol (monoolein, MO) that forms the Pn3m structure with 40% (w/w) hydration at room temperature and supports the gyroid type with lower hydration conditions.[31] The Pn3m and Ia3d cubic phases are preferred by lipid species that support highly negative curvatures, similar to those forming the $H_{II}$ phase.[43] The fact that oxidized DOPE forms an Im3m phase therefore suggests it is less capable of supporting high curvatures than the unoxidized species. Monoolein-based lipid cubic phase structures that are formed *in vitro* usually have unit cell sizes of hundreds of angstroms, an order of magnitude lower than the cubic structures observed in nature.[36] While the double diamond and gyroid cubic phases contain tetrahedral (109.5°) and three-way (120°) water channel junctions, respectively, the Im3m phase contains 90° 6-way junctions and requires less negative curvature.[44] For this reason, Im3m structures are capable of more drastic cell size expansion compared to the other two cubic phases.[43] Anionic lipids and poly(ethylene glycol)-conjugated PE, both allowing for higher levels of headgroup hydration, induce formation of the Im3m phase and drastically increase the lattice parameter of monoolein-based lipid mixtures by approximately 70 Å, from 106 Å for pure monoolein.[31] These additive species form the $L_\alpha$ phase in pure form and thus reduce the magnitude of the negative curvature when mixed with monoolein.[36] Similarly, DOPE acyl tails obtain polar functional groups through oxidation that causes the formerly hydrophobic moiety to migrate closer to the lipid–water interface and results in lipid headgroup area expansion.[27] Certain ternary mixtures of surfactants, water, and oil (similar to oxidation-scission lipid tail fragments) have been shown to support cubic lipid phases.[45,46] We hypothesize that the emergence of mixed subpopulations with different intrinsic curvatures, with the presence of negative curvature species (e.g., DOPE and monoolein) and $L_\alpha$ phase-forming species together, is significant in forming the Im3m phase that is possibly related to optically resolved lattice structures with near-micron spacing. Furthermore, the time-dependent changes in water hydration levels and loss of lipid tail fragments to the aqueous phase can account for the transience of these larger square lattice structures.

### Characterization of lipid geometry.

The oxidation of DOPE results in a mixture of products with increased headgroup areas at the expense of hydrophobic moieties. While DOPE supports the $H_{II}$ phase in water, the hydration of oxidized samples resulted in the formation of $Q_{II}$ (Im3m, confirmed by SAXS

data) and $L_\alpha$ phase structures that are supported by more cylindrical molecules. The deviation of a lipid molecular structure from resembling a cylindrical volume can be described and used to predict the morphological phase it can support. Israelachvili and co-workers[47–49] studied lipid packing of various shapes of molecules and quantified lipid structure with the lipid packing parameter, $\gamma = V/Al$, where $V$ is the volume occupied by the lipid tails, $A$ is the lateral area of the headgroup, and $l$ is the length of the lipid tail region. Cylindrical lipids that support lamellar bilayer formation have $\gamma$ close to unity, while lipids with small head groups ($\gamma > 1$) such as PE lipids form the $H_{II}$ phase. DOPE has the packing parameter $\gamma_{DOPE} = 1.38$, while its PC counterpart more closely resembles a cylindrical volume ($\gamma_{DOPC} = 1.09$).[50]

Here, we aim to estimate the effective packing parameter of the collective oxidized DOPE species from the observed $L_\alpha$ phase morphologies. Kumar[51] has demonstrated that packing parameter is additive in lipids with long chain lengths (10 or more carbon atoms per acyl chain): the effective packing parameter for a mixture of lipid species is the linear combination of the packing parameter of each individual species, weighted by mole fraction. To demonstrate that the calculated effective packing parameter can predict hydrated lipid morphologies, we performed the hydration experiment using samples with varying ratios of DOPE to lyso-PE ($\gamma_{lyso-PE} = 0.5\gamma_{DOPE}$). An 18-carbon, monounsaturated tail lyso-PE species was selected to mimic a truncated-tail DOPE molecule. The increasing molar fractions of lyso-PE were studied to simulate the increase in the extent of oxidation of the DOPE population. The lyso-PE/DOPE films were hydrated with Milli-Q water with $5 \times 10^{-7}$ M lyso-PE (estimated as the critical micelle concentration based on information from Marsh[52]) in solution to minimize dissolution of the surfactant-like lipid from the film. At 100 mol % DOPE ($\gamma = 1.38$), the lipid film showed no significant changes when hydrated. As the fraction of lyso-PE increases, the calculated effective packing parameter decreases. From 40 mol % lyso-PE ($\gamma = 1.10$) upward, tubules and vesicles were present within 5 min into hydration (Figure S7). The calculated packing parameter for this mixture is comparable to that of DOPC that forms the lamellar phase. Thus, we are using this packing parameter value for the transition point where the $L_\alpha$ phase structures appear.

Note that the DOPE/lyso-PE mixtures were diluted with chloroform so that the final concentration before drying on the coverslip was uniformly 0.7 mg DOPE/mL. This is much lower than the 10 mg/mL concentration of the oxidized DOPE samples. We repeated the hydration experiment with oxidized DOPE using 0.7 mg/mL (Figure S8). At this lower lipid amount, the lattice-to-lamellar phase transition occurred more quickly due to increased hydration rates.

As previously described, DOPE was oxidized in 4-h intervals. After each oxidation period, we also analyzed the samples with proton nuclear magnetic resonance ($^1$H NMR) spectroscopy and performed the hydration experiment using 0.05 mg of the original 10 mg samples. The progress of oxidation was measured with the remaining amounts of vinyl protons, estimated by integrating the vinyl proton peak normalized to the area under the glycerol proton peak (highlighted blue and red, respectively, in Figure 5A). The normalized amount of vinyl protons for an ideal nonoxidized DOPE sample is 4. During the oxidation of a monounsaturated lipid such as DOPE, an allylic hydrogen is first abstracted from one of

the lipid tails by a reactive oxygen species. The lipid molecule is left as a carbon-centered radical that reacts with molecular oxygen and another lipid molecule and results with a hydroperoxy group. While the peak for hydroperoxy proton is difficult to isolate in the NMR spectrum, the functional group being adjacent to the double bond causes a downshift of the vinyl peak (from 5.34 ppm to approximately 5.70 ppm, Figure 5B). The scission of the lipid tail with further oxidation eliminates the vinyl peak completely. Thus, integrating the vinyl proton peak of the $^{1}$H NMR spectrum is a reasonable method for determining the fraction of DOPE lipids that is not oxidized.

The progress of oxidation, as followed via the loss of vinyl protons, is shown in Figure 5C. Note that the tail scission step typically yields the aldehyde group that was not represented in the NMR spectra for our system. Comparing the total amounts of lipids oxidized (complementary to the values in Figure 5C) and the amounts of peroxidized lipids (by integrating the shifted vinyl peaks), peroxidation does not account for all lipids oxidized (Figure S9). As seen from our previous work in oxidizing DOPC,[27] tail scission occurred with further oxidation of the peroxidized product. Furthermore, in comparison to DOPC, the aldehyde groups formed with oxidation of PE can participate in a condensation reaction with the amine group of the PE headgroup to yield fluorescent Schiff bases. Fluorescence spectroscopy measurements of oxidized DOPE and nonoxidized DOPE combined with an aldehyde species, with DOPC samples as controls, confirms Schiff base formation (Figure S10) and therefore strengthens our speculation of DOPE tail scission during oxidation.

Accompanying hydration experiments of samples after each set of NMR scans showed that oxidized DOPE films resembled that of nonoxidized DOPE, after up to 20 h of air/heat treatment. However, the lamellar phase and lattice structures emerged after a total of 24 h of oxidation (e.g., Figure 1), where ± 1.66% (standard deviation from 3 samples) of the vinyl protons were present. We noted that the stock DOPE sample (with 0 h of intentional oxidation) started with 96.83 ± 1.50% vinyl protons, and this was factored in for the calculation of the effective packing parameter. This readjusted the effective packing parameter of the 60 mol % DOPE/40 mol % lyso-PE sample to 1.090 ± 0.014. In order for the 24-h oxidized DOPE sample to have the same effective packing parameter, the average packing parameter value for the oxidized lipid portion was calculated to be 0.657 ± 0.069. This suggests that the inverted wedge or cone characteristic of an “average” oxidized DOPE molecule therefore has greater deviation from cylindrical than the original wedge shape, and in the opposite direction, of nonoxidized DOPE (i.e., $\gamma_{\mathrm{oxDOPE}} < 1/\gamma_{\mathrm{DOPE}}$).

## CONCLUSIONS

Oxidative stress is a common mechanism of cellular damage that leads to pathology in a whole host of human diseases, including cancer, atherosclerosis, and neurodegeneration.[24,53] Disruption of normal metabolic processes in the mitochondria and endoplasmic reticulum leads to formation of byproducts that either contain or lead to downstream production of reactive oxygen species.[24] Cellular membranes are especially susceptible to oxidative damage due to predominance of fatty acid chains. As a result, it is essential to understand the effects of lipid oxidation on the topology of cellular membranes. The molecular structure of PE lipids is central to their role in dynamic cellular processes where high curvature is

involved. They serve as ideal prototypical lipids for studies of oxidation-induced changes in molecular shape and intrinsic curvature.[3,4,20] In this study, we demonstrate that molecular alterations resulting from oxidation of PE lipids lead to drastic changes in the phase behavior of lipid membranes. The oxidation of a lipid molecule changes the ratio between its head and tail group areas. For DOPE, and based on this ratio, we have estimated that the resulting oxidation products incur a molecular intrinsic curvature sign change and, on average, contain a higher magnitude of curvature than the nonoxidized species. SAXS results show that the combined presences of DOPE and its oxidization products induced structures rich in negative Gaussian curvature, which is a necessary ingredient in many membrane permeation events.[54] The pure DOPE composition used in our study is not identical to what is found in typical mammalian membranes, which contain PE lipids in coexistence with a distribution of other lipid species. The use of pure DOPE in a model system, however, limited the number of possible oxidation products and allowed us to identify a potentially important structural tendency of the PE subphase to change intrinsic curvature upon oxidation.

PE lipids are unique when compared to the more predominant PC phospholipids. For any lipid acyl tail, oxidation can result in the addition of a hydroperoxy group and the formation of an aldehyde group with tail scission. The amine group of the PE lipid headgroup can participate in a condensation reaction with this aldehyde group to form a fluorescent Schiff base product.[55–57] We hypothesize that it is this last, high-molecular weight product that provides the rigidity required to minimize thermal fluctuations for stabilizing such large lattice spacing.

## Supplementary Material

Refer to Web version on PubMed Central for supplementary material.

## ACKNOWLEDGMENTS

The authors value input from Dr. Vadim Cherezov. NMR spectroscopy work was performed at the University of Southern California (USC) Center of Excellence for Molecular Characterization. Fluorescence spectroscopy experiments were performed at the USC Center of Excellence in NanoBiophysics with advisement from Dr. Shuxing Li. SAXS experiments were performed at the Stanford Synchrotron Radiation Lightsource facility. This work was funded by the Office of Naval Research (award N000141210620).

## REFERENCES

(1). Singer SJ; Nicolson GL Fluid mosaic model of structures of cell membranes. Science 1972, 175, 720–731. [PubMed: 4333397]

(2). Seddon JM Structure of the inverted hexagonal (HII) phase, and non-lamellar phase transitions of lipids. Biochim. Biophys. Acta, Rev. Biomembr 1990, 1031, 1–69.

(3). Ellens H; Siegel DP; Alford D; Yeagle PL; Boni L; Lis LJ; Quinn PJ; Bentz J Membrane fusion and inverted phases. Biochemistry 1989, 28, 3692–3703. [PubMed: 2751990]

(4). Burger KNJ Greasing membrane fusion and fission machineries. Traffic 2000, 1, 605–613. [PubMed: 11208148]

(5). Ostrowski SG; Van Bell CT; Winograd N; Ewing AG Mass spectrometric imaging of highly curved membranes during Tetrahymena mating. Science 2004, 305, 71–73. [PubMed: 15232100]

(6). Hyde ST Bicontinuous structures in lyotropic liquid crystals and crystalline hyperbolic surfaces. Curr. Opin. Solid State Mater. Sci 1996, 1, 653–662.

(7). Larsson K Cubic lipid-water phases: structures and biomembrane aspects. J. Phys. Chem 1989, 93, 7304–7314.

(8). Landh T From entangled membranes to eclectic morphologies: cubic membranes as subcellular space organizers. FEBS Lett 1995, 369, 13–17. [PubMed: 7641875]

(9). Jouhet J Importance of the hexagonal lipid phase in biological membrane organization. Front. Plant Sci 2013, 4, 494. [PubMed: 24348497]

(10). Schaff Z; Lapis K; Grimley PM Undulating membraneous structures associated with the endoplasmic reticulum in tumour cells. Int. J. Cancer 1976, 18, 697–702. [PubMed: 186416]

(11). Grimley PM; Schaff Z Significance of tubuloreticular inclusions in the pathobiology of human diseases. Pathobiol. Annu 1976, 6, 221–257. [PubMed: 798160]

(12). Almsherqi ZA; Kohlwein SD; Deng Y Cubic membranes: a legend beyond the Flatland of cell membrane organization. J. Cell Biol 2006, 173, 839–844. [PubMed: 16785319]

(13). Goldsmith CS; Tatti KM; Ksiazek TG; Rollin PE; Comer JA; Lee WW; Rota PA; Bankamp B; Bellini WJ; Zaki SR Ultrastructural characterization of SARS coronavirus. Emerging Infect. Dis 2004, 10, 320–326. [PubMed: 15030705]

(14). Deng Y; Kohlwein SD; Mannella CA Fasting induces cyanide-resistant respiration and oxidative stress in the amoeba Chaos carolinensis: implications for the cubic structural transition in mitochondrial membranes. Protoplasma 2002, 219, 160–167. [PubMed: 12099216]

(15). Griffing LR Networking in the endoplasmic reticulum. Biochem. Soc. Trans 2010, 38, 747–753. [PubMed: 20491660]

(16). van Venetie R; Verkleij AJ Possible role of non-bilayer lipids in the structure of mitochondria. A freeze-fracture electron microscopy study. Biochim. Biophys. Acta, Biomembr 1982, 692, 397–405.

(17). Daum G; Vance JE Import of lipids into mitochondria. Prog. Lipid Res 1997, 36, 103–130. [PubMed: 9624424]

(18). Ardail D; Privat JP; Egret-Charlier M; Levrat C; Lerme F; Louisot P Mitochondrial contact sites. Lipid composition and dynamics. J. Biol. Chem 1990, 265, 18797–18802. [PubMed: 2172233]

(19). Horvath SE; Daum G Lipids of mitochondria. Prog. Lipid Res 2013, 52, 590–614. [PubMed: 24007978]

(20). Emoto K; Kobayashi T; Yamaji A; Aizawa H; Yahara I; Inoue K; Umeda M Redistribution of phosphatidylethanolamine at the cleavage furrow of dividing cells during cytokinesis. Proc. Natl. Acad. Sci. U. S. A 1996, 93, 12867–12872. [PubMed: 8917511]

(21). Gagne J; Stamatatos L; Diacovo T; Hui SW; Yeagle PL; Silvius JR Physical properties and surface interactions of bilayer membranes containing N-methylated phosphatidylethanolamines. Biochemistry 1985, 24, 4400–4408. [PubMed: 4052405]

(22). Gruner SM Intrinsic curvature hypothesis for biomembrane lipid composition: a role for nonbilayer lipids. Proc. Natl. Acad. Sci. U. S. A 1985, 82, 3665–3669. [PubMed: 3858841]

(23). Erbes J; Czeslik C; Hahn W; Winter R; Rappolt M; Rapp G On the existence of bicontinuous cubic phases in dioleoylphosphatidylethanolamine. Ber. Bunsenges. Phys. Chem 1994, 98, 1287–1293.

(24). Halliwell B Oxidative stress and neurodegeneration: where are we now? J. Neurochem 2006, 97, 1634–1658. [PubMed: 16805774]

(25). Newmeyer DD; Ferguson-Miller S Mitochondria: releasing power for life and unleashing the machineries of death. Cell 2003, 112, 481–490. [PubMed: 12600312]

(26). Smith WL; Murphy RC Oxidized lipids formed non-enzymatically by reactive oxygen species. J. Biol. Chem 2008, 283, 15513–15514. [PubMed: 18285325]

(27). Sankhagowit S; Wu S-H; Biswas R; Riche CT; Povinelli ML; Malmstadt N The dynamics of giant unilamellar vesicle oxidation probed by morphological transitions. Biochim. Biophys. Acta, Biomembr 2014, 1838, 2615–2624.

(28). Runas KA; Malmstadt N Low levels of lipid oxidation radically increase the passive permeability of lipid bilayers. Soft Matter 2015, 11, 499–505. [PubMed: 25415555]

(29). Schmidt NW; Wong GCL Antimicrobial peptides and induced membrane curvature: Geometry, coordination chemistry, and molecular engineering. Curr. Opin. Solid State Mater. Sci 2013, 17, 151–163. [PubMed: 24778573]

(30). Landau EM; Rosenbusch JP Lipidic cubic phases: A novel concept for the crystallization of membrane proteins. Proc. Natl. Acad. Sci. U. S. A 1996, 93, 14532–14535. [PubMed: 8962086]

(31). Cherezov V; Clogston J; Misquitta Y; Abdel-Gawad W; Caffrey M Membrane protein crystallization in meso: lipid type-tailoring of the cubic phase. Biophys. J 2002, 83, 3393–3407. [PubMed: 12496106]

(32). Shyamsunder E; Gruner SM; Tate MW; Turner DC; So PTC; Tilcock CPS Observation of inverted cubic phase in hydrated dioleoylphosphatidylethanolamine membranes. Biochemistry 1988, 27, 2332–2336. [PubMed: 3382626]

(33). Tenchov B; Koynova R Cubic phases in membrane lipids. Eur. Biophys. J 2012, 41, 841–850. [PubMed: 22584384]

(34). Angelov B; Angelova A; Ollivon M; Bourgaux C; Campitelli A Diamond-type lipid cubic phase with large water channels. J. Am. Chem. Soc 2003, 125, 7188–7189. [PubMed: 12797787]

(35). Johnsson M; Barauskas J; Tiberg F Cubic phases and cubic phase dispersions in a phospholipid-based system. J. Am. Chem. Soc 2005, 127, 1076–1077. [PubMed: 15669827]

(36). Tyler AII; Barriga HMG; Parsons ES; McCarthy NLC; Ces O; Law RV; Seddon JM; Brooks NJ Electrostatic swelling of bicontinuous cubic lipid phases. Soft Matter 2015, 11, 3279–3286. [PubMed: 25790335]

(37). Deng Y; Marko M; Buttle KF; Leith A; Mieczkowski M; Mannella CA Cubic membrane structure in amoeba (Chaos carolinensis) mitochondria determined by electron microscopic tomography. J. Struct. Biol 1999, 127, 231–239. [PubMed: 10544048]

(38). Wiener MC; White SH Structure of a fluid dioleoylphosphatidylcholine bilayer determined by joint refinement of x-ray and neutron-diffraction data 0.3. Complete structure. Biophys. J 1992, 61, 434–447. [PubMed: 1547331]

(39). Tristram-Nagle S; Petrache HI; Nagle JF Structure and interactions of fully hydrated dioleoylphosphatidylcholine bilayers. Biophys. J 1998, 75, 917–925. [PubMed: 9675192]

(40). Schmidt NW; Lis M; Zhao K; Lai GH; Alexandrova AN; Tew GN; Wong GCL Molecular basis for nanoscopic membrane curvature generation from quantum mechanical models and synthetic transporter sequences. J. Am. Chem. Soc 2012, 134, 19207–19216. [PubMed: 23061419]

(41). Schmidt NW; Mishra A; Wang J; DeGrado WF; Wong GCL Influenza virus A M2 protein generates negative Gaussian membrane curvature necessary for budding and scission. J. Am. Chem. Soc 2013, 135, 13710–13719. [PubMed: 23962302]

(42). Harper PE; Mannock DA; Lewis R; McElhaney RN; Gruner SM X-ray diffraction structures of some phosphatidylethanolamine lamellar and inverted hexagonal phases. Biophys. J 2001, 81, 2693–2706. [PubMed: 11606282]

(43). Kulkarni CV; Tang T-Y; Seddon AM; Seddon JM; Ces O; Templer RH Engineering bicontinuous cubic structures at the nanoscale-the role of chain splay. Soft Matter 2010, 6, 3191–3194.

(44). Kulkarni CV; Wachter W; Iglesias-Salto G; Engelskirchen S; Ahualli S Monoolein: a magic lipid? Phys. Chem. Chem. Phys 2011, 13, 3004–3021. [PubMed: 21183976]

(45). Li X Kunieda H. Formation of cubic-phase microemulsions with anionic and cationic surfactants at equal amounts of oil and water. Colloid Interface Sci 2000, 231, 143–151.

(46). Leaver MS; Olsson U; Wennerstrom H; Strey R; Wurz U Phase behaviour and structure in a non-ionic surfactant-oil-water mixture. J. Chem. Soc., Faraday Trans 1995, 91, 4269–4274.

(47). Israelachvili JN; Mitchell DJ; Ninham BW Theory of self-assembly of hydrocarbon amphiphiles into micelles and bilayers. J. Chem. Soc., Faraday Trans. 2 1976, 72, 1525–1568.

(48). Israelachvili JN; Mitchell DJ; Ninham BW Theory of self-assembly of lipid bilayers and vesicles. Biochim. Biophys. Acta, Biomembr 1977, 470, 185–201.

(49). Israelachvili JN; Marcelja S; Horn RG Physical principles of membrane organization. Q. Rev. Biophys 1980, 13, 121–200. [PubMed: 7015403]

(50). Marsh D Nonlamellar packing parameters for diacylglycerols. Biophys. J 1997, 72, 2834–2836. [PubMed: 9168057]

(51). Kumar VV Complementary molecular shapes and additivity of the packing parameter of lipids. Proc. Natl. Acad. Sci. U. S. A 1991, 88, 444–448. [PubMed: 1988944]

(52). Marsh D Handbook of Lipid Bilayers, 1st Edition; CRC Press: 1990.

(53). Lee SE; Park YS Role of lipid peroxidation-derived alpha, beta-unsaturated aldehydes in vascular dysfunction. Oxid. Med. Cell. Longevity 2013.

(54). Schmidt NW; Mishra A; Lai GH; Davis M; Sanders LK ; Dat T; Garcia A; Tai KP; McCray J; Paul B; Ouellette AJ; Selsted ME; Wong GCL Criterion for amino acid composition of defensins and antimicrobial peptides based on geometry of membrane destabilization. J. Am. Chem. Soc 2011, 133, 6720–6727. [PubMed: 21473577]

(55). Bhuyan DK; Master RWP; Bhuyan KC Crosslinking of aminophospholipids in cellular membranes of lens by oxidative stress in vitro. Biochim. Biophys. Acta, Biomembr 1996, 1285, 21–28.

(56). Bidlack WR; Tappel AL Fluorescent products of phospholipids during lipid peroxidation. Lipids 1973, 8, 203–207. [PubMed: 4695132]

(57). Hermetter A; Kopec W; Khandelia H Conformations of double-headed, triple-tailed phospholipid oxidation lipid products in model membranes. Biochim. Biophys. Acta, Biomembr 2013, 1828, 1700–1706.

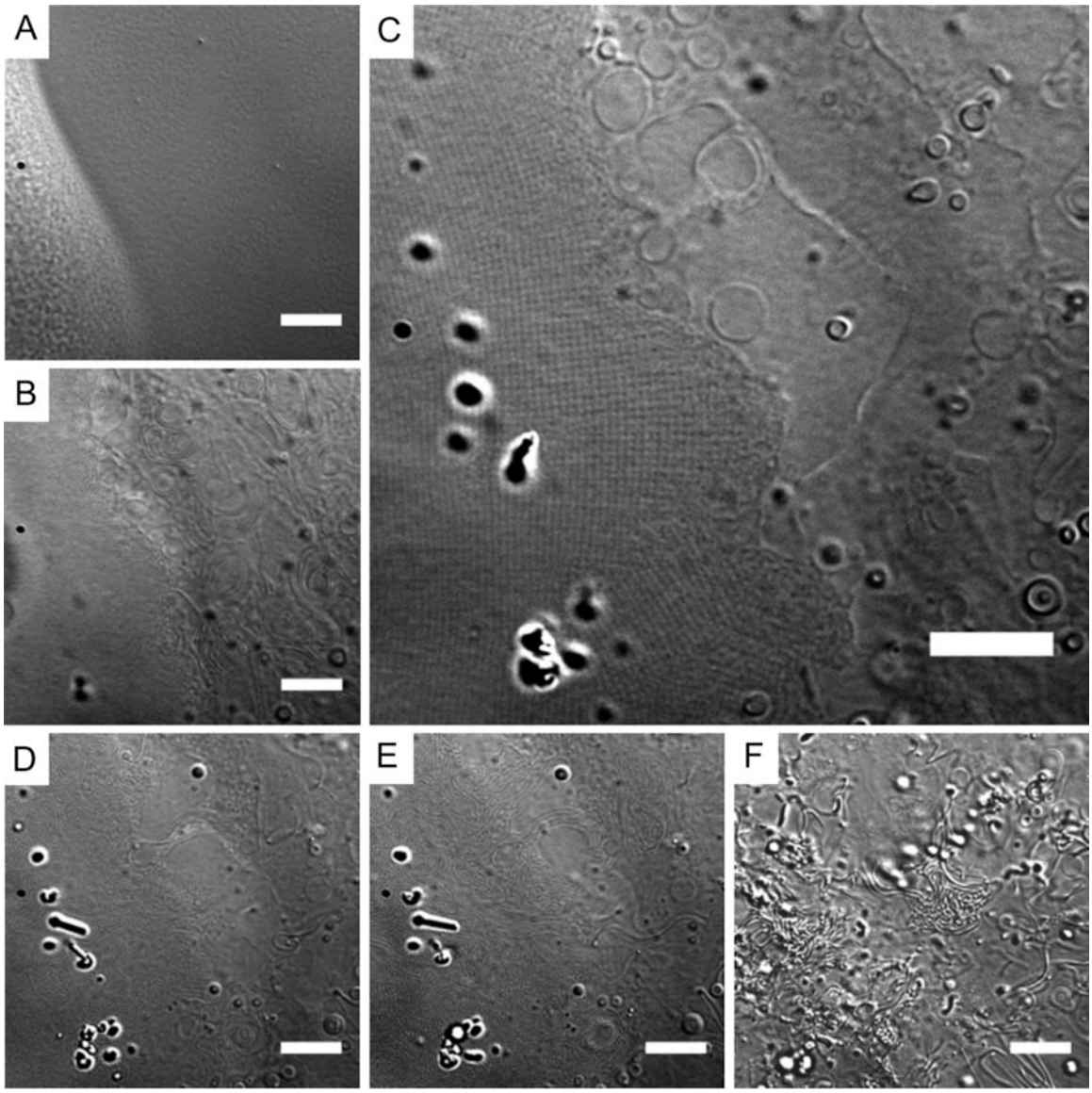


**Figure 1.**

Hydrated 24-h oxidized DOPE lipid. (A) Dried lipid film. (B–F) Hydrated lipid film: (B) 20 s and (C) 4 min after addition of water, showing a lattice structure (left side) and the lamellar phase as vesicles and tubules (right side), followed by transition from the lattice structure into tubules (D) 7 min and (E) 8 min after hydration. (F) At 10 min after hydration, tubules lifted upward and therefore appeared at higher contrast. Scale bars = 10 $\mu$m.

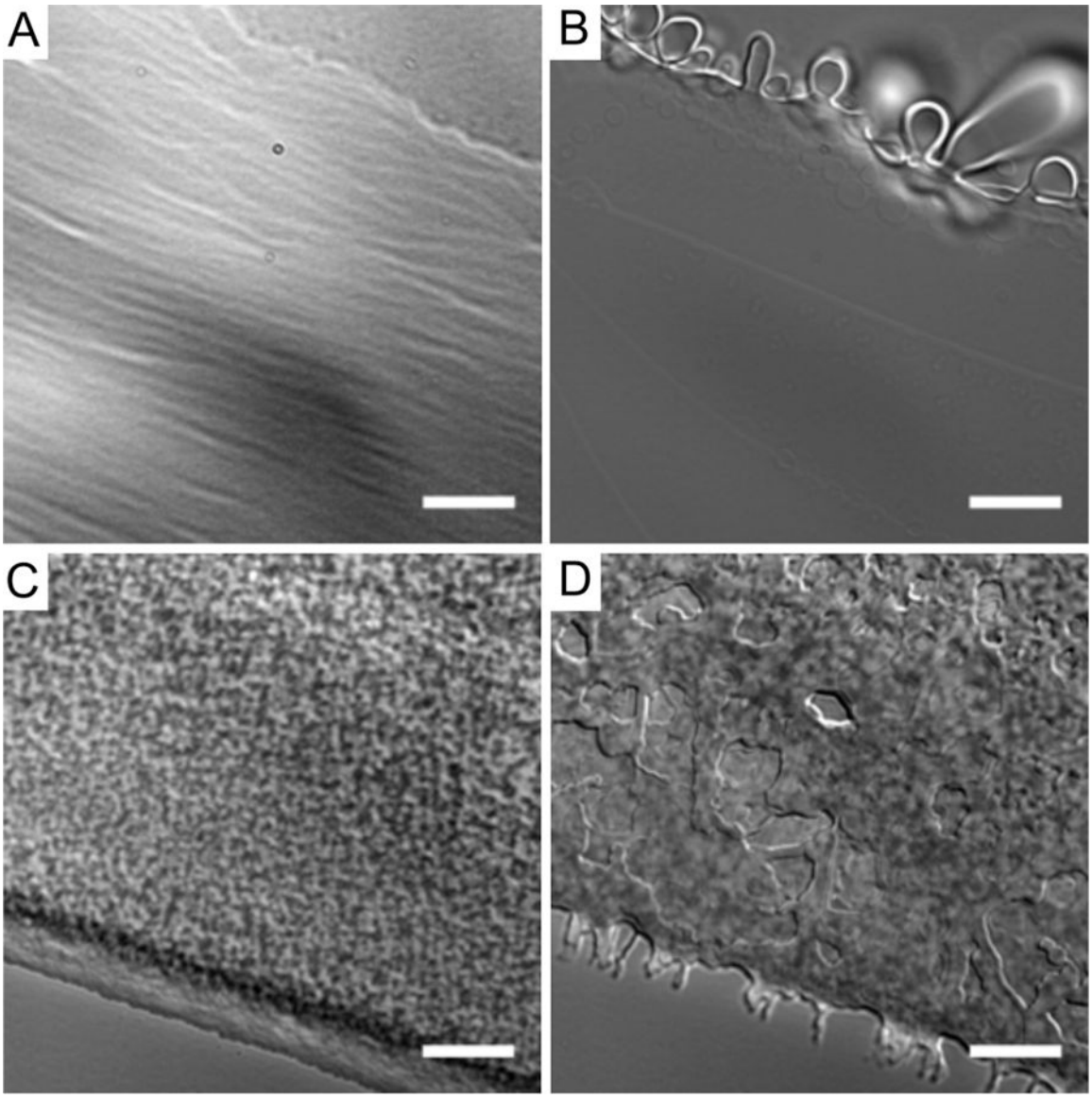


**Figure 2.**

Comparison of lamellar and nonlamellar phases in water. DOPC ($L_\alpha$ phase): (A) dried and (B) 5 min after hydration. DOPE ($H_{II}$ phase at room temperature): (C) dried and (D) 5 min after hydration. Scale bars = 10 $\mu$m.

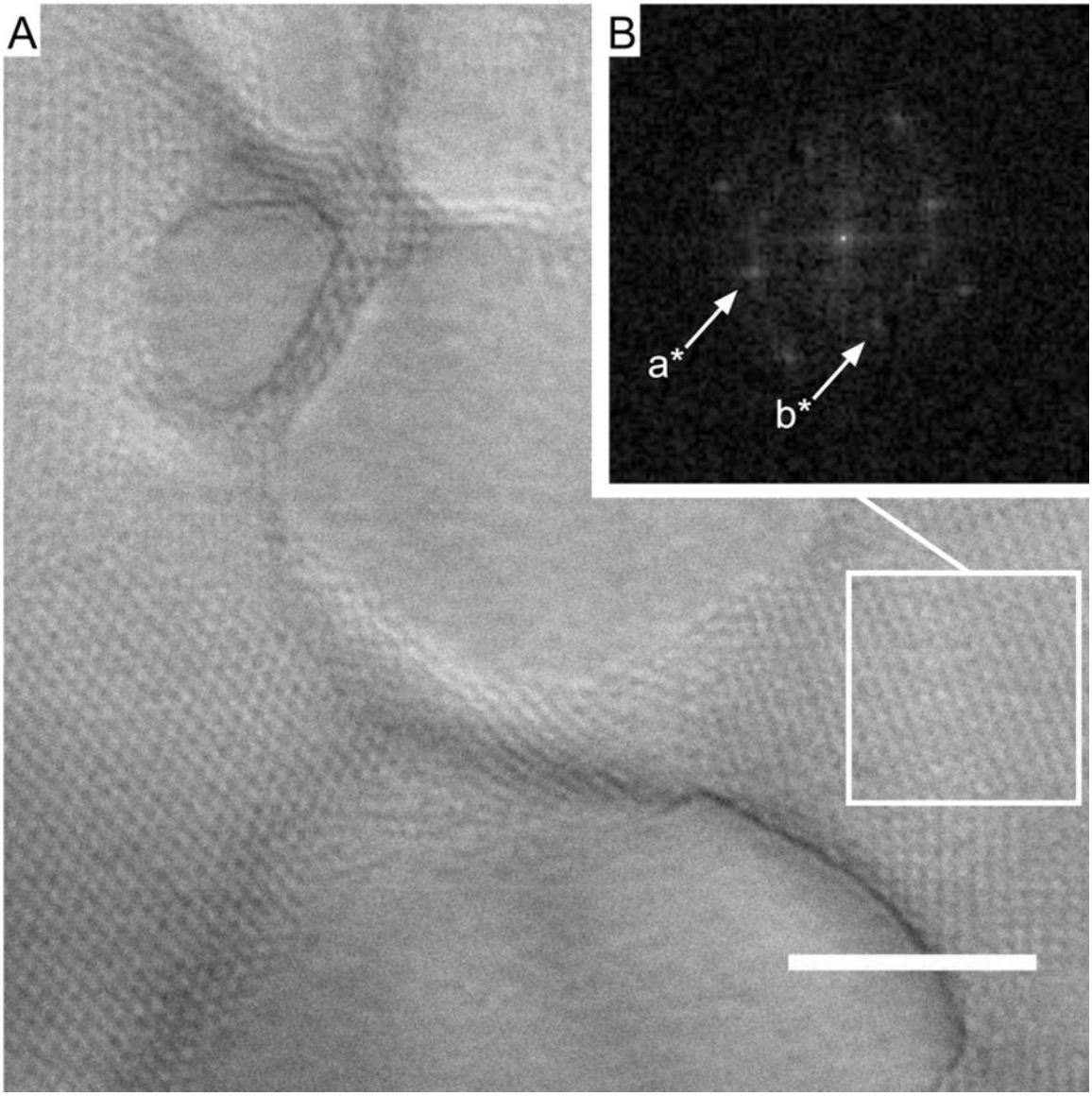


**Figure 3.**

(A) Hydrated 24-h oxidized DOPE showing the cropped section analyzed through FFT (boxed). Scale bar = 10 $\mu$m. (B) 2-D fast Fourier transform of a square pattern; the indicated reflections correspond to reciprocal lattice vectors $a^*$ and $b^*$. The angle between the reflections is 90°, and the lattice parameters are $a = 628 \pm 202$ nm and $b = 628 \pm 217$ nm.

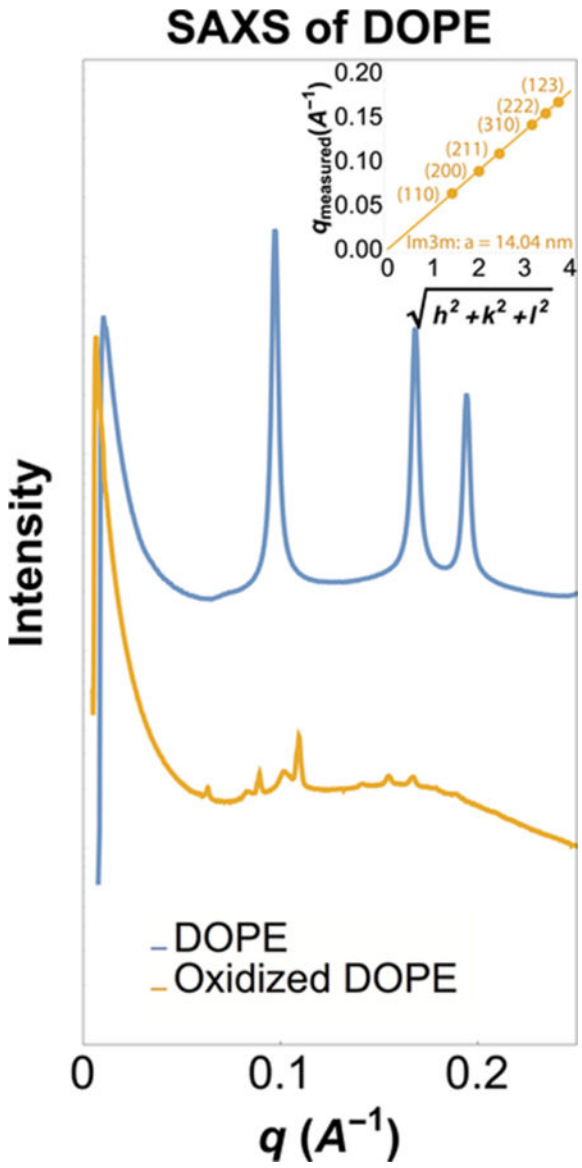


**Figure 4.**

SAXS results for oxidized DOPE showing the Im3m phase with $a$ = 14.04 nm (yellow) and nonoxidized DOPE showing the inverted hexagonal phase (blue).

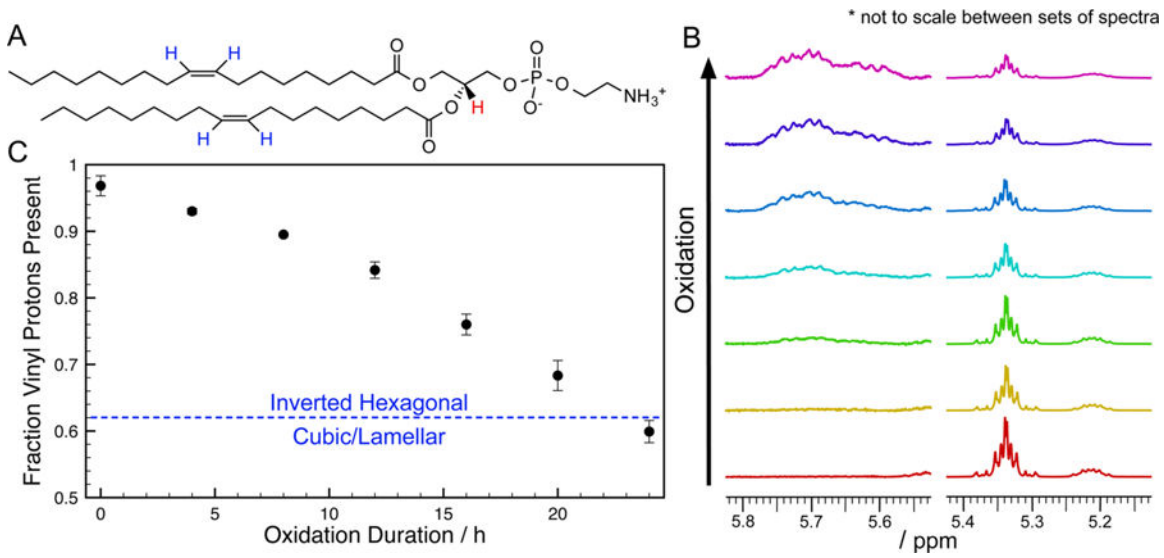


**Figure 5.**

Estimating the extent of oxidation with $^{1}$H NMR. (A) Molecular structure of DOPE showing vinyl protons (blue) and the glycerol proton (red). (B) $^{1}$H NMR spectra of oxidized samples of DOPE showing the glycerol (5.22 ppm) and vinyl (5.34 ppm) proton peaks, as well as the emergence of the shifted vinyl peak (~5.70 ppm) due to the substitution of an allylic proton with a hydroperoxy group. The bottom spectra (red) are of the stock, nonoxidized sample, and each successive spectrum was taken after a cycle of evaporating chloroform, heating at 50 °C for 4 h, and redissolving in deuterated chloroform for 1H NMR spectroscopy. (C) Progression of DOPE oxidation with air and heat exposure duration, measured as the integration of the vinyl proton peak with respect to the glycerol proton peak from the $^{1}$H NMR spectrum obtained at each time point. Each data point is averaged from three samples oxidized in parallel, with the error bar representing the standard deviation.